GEOPHYSICAL RESEARCH LETTERS, VOL. 34, L13701, doi:10.1029/2007GL030017, 2007

Seawater isotope constraints on tropical hydrology during the Holocene

Delia W. Oppo,[1] Gavin A. Schmidt,[2] and Allegra N. LeGrande[2]

Received 15 March 2007; revised 8 May 2007; accepted 15 May 2007; published 3 July 2007.

[1] Paleoceanographic data from the low latitude Pacific Ocean provides evidence of changes in the freshwater budget and redistribution of freshwater within the basin during the Holocene. Reconstructed Holocene seawater δ^{18}O changes compare favorably to differences predicted between climate simulations for the middle Holocene (MH) and for the pre-Industrial late Holocene (LH). The model simulations demonstrate that changes in the tropical hydrologic cycle affect the relationship between δ^{18}Osw and surface salinity, and allow, for the first time, quantitative estimates of western Pacific salinity change during the Holocene. The simulations suggest that during the MH, the mean salinity of the Pacific was higher because less water vapor was transported from the Atlantic Ocean and more was transported to the Indian Ocean. The salinity of the western Pacific was enhanced further due both to the greater advection of salt to the region by ocean currents and to an increase in continental precipitation at the expense of maritime precipitation, the latter a consequence of the stronger Asian summer monsoon. **Citation:** Oppo, D. W., G. A. Schmidt, and A. N. LeGrande (2007), Seawater isotope constraints on tropical hydrology during the Holocene, *Geophys. Res. Lett.*, *34*, L13701, doi:10.1029/2007GL030017.

1. Introduction

[2] Perihelion occurred in boreal summer during the early Holocene, shifting to boreal winter over the course of the Holocene [*Berger*, 1978]. Consequently, the amplitude of the seasonal cycle of incoming radiation in the northern hemisphere was greater during the early and middle Holocene than today, and tropical climate systems experienced significant reorganization. For example, during the mid-Holocene, the Asian summer monsoons were stronger [e.g., *Fleitmann et al.*, 2003] and El Niño events were weaker and/or less frequent [*Koutavas et al.*, 2006; *Moy et al.*, 2002]. Hydrologic changes were recorded in climate archives such as speleothems [e.g., *Fleitmann et al.*, 2003; *Holmgren et al.*, 2003; *Wang et al.*, 2005], groundwater [e.g., *Gasse*, 2000], and ice cores [e.g., *Thompson and Davis*, 2005] as temporal and spatial variations in water isotopes.

[3] Hydrologic changes impacted continental moisture balance, but their effect on the surface salinity of the ocean is poorly constrained. Yet, surface salinity distribution is a primary indicator of atmospheric vapor transport and precipitation, and both affects and provides a major control on the thermohaline circulation [e.g., *Schmittner and Clement*, 2002; *Schmidt et al.*, 2004]. A direct paleoceanographic proxy for surface salinity does not exist, but seawater δ^{18}O (δ^{18}Osw) reconstructions, when coupled with isotope climate model simulations, can constrain changes in the tropical hydrologic cycle, and potentially, salinity changes. In this study, we analyze published foraminiferal geochemical data from the low-latitude Pacific Ocean [*Koutavas et al.*, 2002; *Koutavas et al.*, 2006; *Lea et al.*, 2000; *Lea et al.*, 2006; *Spero and Lea*, 2003; *Stott et al.*, 2004; *Y. Sun et al.*, 2005; *Visser et al.*, 2003] to assess δ^{18}Osw change since the mid-Holocene and compare it to an isotope enabled climate model [*Schmidt et al.*, 2007].

2. Methods

[4] The δ^{18}O values of the calcite shells of planktonic foraminifera (δ^{18}Oc) are a function of both δ^{18}Osw and temperature. Since calcification temperature can be estimated by Mg/Ca paleothermometry [e.g., *Dekens et al.*, 2002], the temperature component of δ^{18}Oc can be estimated and δ^{18}Osw derived [*Bemis et al.*, 1998]. We compile Mg/Ca-based sea surface temperature (SST) estimates and δ^{18}Oc data of shells of the mixed-layer planktonic foraminifera *Globigerinoides ruber* (*G. ruber*) and *G. sacculifer* and, if not already published, compute δ^{18}Osw using the low light equation of *Orbulina universa* determined from culture [*Bemis et al.*, 1998]. All authors apply equations that result in a 1°C SST increase for a 9% exponential increase in Mg/Ca. Applying a 7% exponential increase instead [*McConnell and Thunell*, 2005] increases the amplitude of SST change.

[5] To estimate MH and LH differences, we average data over 3-kyr intervals centered at 6 ka (MH) and 1.5 ka (LH), thereby smoothing over millennial and centennial variability. We apply Student t-tests to evaluate the significance of the differences between the MH and LH means (Table 1). For the two western Pacific cores with the highest resolution [*Stott et al.*, 2004], results are similar using 1-kyr-long and 3-kyr-long time slices (not shown), giving us confidence that the 3-kyr time slices provide reasonable estimates of MH-LH differences. Only data from cores with more than one Mg/Ca and δ^{18}Oc data point in both time slices are considered. MH and LH means are provided in the auxiliary material (Table S1).[1]

[6] The MH-LH data differences are compared to simulations from the Goddard Institute of Space Studies ModelE-R [*Schmidt et al.*, 2007], a coupled ocean-atmosphere general

[1]Department of Geology and Geophysics, Woods Hole Oceanographic Institution, Woods Hole, Massachusetts, USA.
[2]NASA Goddard Institute for Space Studies and Center for Climate Systems Research, Columbia University, New York, New York, USA.

0094-8276/07/2007GL030017$05.00

[1]Auxiliary material data sets are available at ftp://ftp.agu.org/apend/gl/2007gl030017. Other auxiliary material files are in the HTML.

Table 1. Data Differences Between the MH and LH Time Slices[a]

Core	Latitude	Longitude	6K−0K δ^{18}Oc, ‰	P	6K−0K SST, °C	P	6K−0K δ^{18}Osw, ‰	P
				Eastern Pacific				
TR163-19[b,c]	2.26	−90.95	0.03	0.8155	0.5	0.349	0.07	0.751
V21-30 (G. sacc.)[d]	−1.22	−89.68	0.28	**0.0004**	−0.6	**0.014**	0.17	**0.041**
V21-30[e]	−1.22	−89.68	0.18	**0.0097**	−0.4	0.1323	0.09	0.242
TR163-22[f]	0.515	−92.4	0.11	0.2859	−0.2	0.2986	−0.15	0.228
				Western Pacific				
MD98-2181[g]	6.3	125.83	0.14	**<0.0001**	0.5	**<0.0001**	0.28	**<0.0001**
MD98-2176[g]	−5	124	0.17	**<0.0001**	0.4	**<0.0001**	0.26	**<0.0001**
MD98-2170[g]	−11	134	0.05	0.4149	0.1	0.5594	0.05	0.218
MD98-2162[h]	−4.69	117.9	−0.04	0.7354	0.1	0.8689	−0.02	0.869
A7[i]	27.82	126.98	0.29	**0.0005**	−0.5	**0.008**	0.18	**0.011**

[a]The Student t-test probability that the means are not different from zero (P) is given for each.
[b]*Lea et al.* [2000].
[c]*Spero and Lea* [2003].
[d]*Koutavas et al.* [2002].
[e]*Koutavas et al.* [2006].
[f]*Lea et al.* [2006].
[g]*Stott et al.* [2004].
[h]*Visser et al.* [2003].
[i]*Y. Sun et al.* [2005].

circulation model that tracks water isotope tracers throughout the hydrologic cycle. The differences between the 6 ka (MH) and Pre-Industrial Late Holocene (LH) simulations result from prescribed changes in orbital forcing and small changes in greenhouse gas concentrations.

3. Results

[7] MH-LH δ^{18}Osw differences are significant in four cores, three from the western Pacific and one from the eastern Pacific. Data from two cores in the tropical western Pacific suggest MH δ^{18}Osw was ∼0.3‰ higher than the LH. The increase was slightly less (∼0.2‰) at the subtropical western Pacific site. Higher mid-Holocene δ^{18}Osw has also been inferred from western Pacific coral records [e.g., *Gagan et al.*, 1998; *D. Sun et al.*, 2005]. Only one of four records from the eastern tropical Pacific suggests higher MH than LH δ^{18}Osw, whereas the three other records suggest no δ^{18}Osw change.

[8] The model simulations suggest the largest MH-LH δ^{18}Osw and salinity changes occurred in the western Pacific warm pool (Figures 1a and 1b), where the data also suggest the largest changes. Where the data suggest little or uncertain change, like the eastern tropical Pacific and southwestern Indonesia, the model also simulates little to no change. In the western tropical Pacific, the model differences are smaller, but consistent in sign, with those suggested by the data (Table 1). A comparison of MH-LH model anomalies in the δ^{18}O of precipitation (Figures 1e and 1f) to δ^{18}O change estimated from tropical terrestrial archives also suggests that the model simulations capture the essential features of the tropical hydrological cycle and associated water isotope processes, with lower Holocene δ^{18}O values in Asia [*Fleitmann et al.*, 2003; *Thompson and Davis*, 2005; *Wang et al.*, 2005], higher values in Namibia [*Gasse*, 2000], and little or no change in South Africa [*Holmgren et al.*, 2003] and the Andes [*Thompson and Davis*, 2005].

[9] The model simulations of tropical Pacific salinity changes are consistent with one previous study [*Kitoh and Murakami*, 2002] but not another [*Abram et al.*, 2007]. The differences may be driven by different responses of SST in the models (Appendix). The δ^{18}Osw and surface salinity anomalies are similar for boreal summer and winter (not shown). The seasonal differences are small because ocean currents tend to homogenize the regionally patchy seasonal precipitation anomalies (Figures 1c and 1d), resulting in anomalies that have a broad spatial scale. Thus our data-model comparison does not depend significantly on the season of foraminifer calcification.

4. The δ^{18}Osw-Salinity Relationship

[10] Previous studies used modern regional, linear relationships between δ^{18}Osw and salinity to estimate past tropical Pacific salinity change [e.g., *Stott et al.*, 2004]. Our model simulations including both salinity and δ^{18}Osw can help evaluate the assumption of an invariant relationship during the Holocene [*Schmidt et al.*, 2007].

[11] Assuming that the spatial relationship seen today [*LeGrande and Schmidt*, 2006] between surface salinity and δ^{18}Osw in the western tropical Pacific (0.3‰/psu) is valid for changes on orbital timescales, the inferred salinity change corresponding to the ∼0.3‰ higher MH δ^{18}Osw is ∼0.9 psu. In the model, the MH-LH δ^{18}Osw changes are more modest (0.07 and 0.16‰, for MD98-2176 and MD98-2181, respectively) than inferred from the sediment cores. Corresponding model salinity changes (0.17 and 0.29 psu, respectively) are ∼75 and 55% of that inferred by applying the modern spatial relationship to the simulated δ^{18}Osw differences (0.23 and 0.53 psu, respectively). Thus the model suggests that the relationship between salinity and δ^{18}Osw in the western tropical Pacific was different during the MH [*Schmidt et al.*, 2007]. Applying the modelled relationships to the sediment data would imply a smaller salinity change (∼0.5 to 0.7 psu) for the ∼0.3‰ δ^{18}Osw observations, rather than the 0.9 psu estimated from the modern spatial relationship.

5. Mechanisms of δ^{18}Osw and Salinity Change

[12] Since the tropical water cycle is largely closed, with little export to higher latitudes, the modern and MH spatial slope of the δ^{18}Osw-salinity relationship is relatively shal-

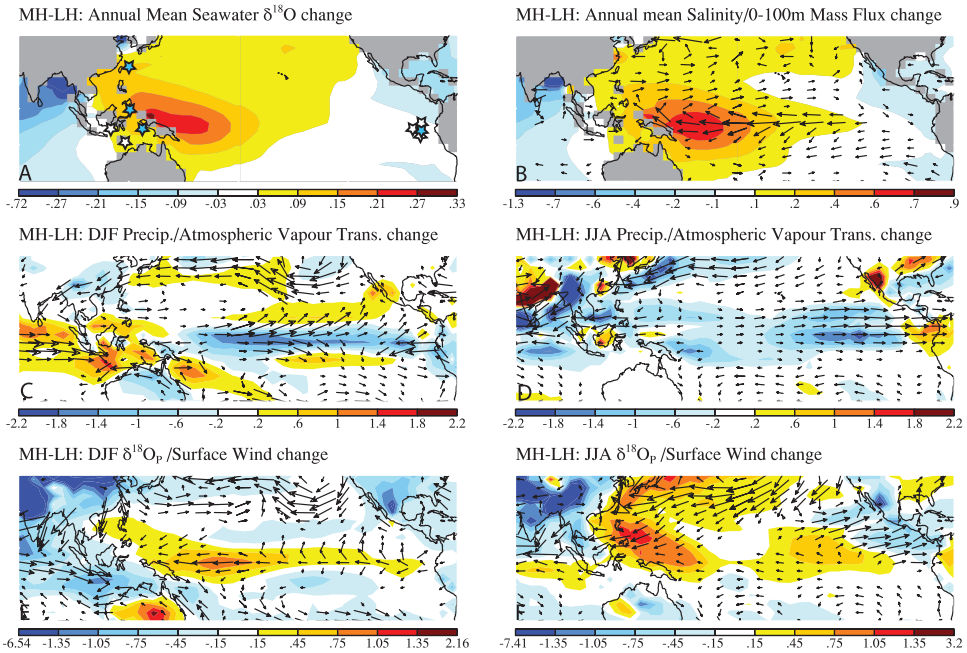

Figure 1. Mean differences between the MH and LH model simulations. (a) Mean annual δ^{18}Osw. (b) Mean annual surface salinity (colors) and 0–100 m mass flux change (arrows). (c) Boreal winter (December, January, February mean) precipitation (color) and water vapor transport (arrows). (d) Boreal summer (June, July, August mean) precipitation (color) and water vapor transport (arrows). (e) Boreal winter δ^{18}O of precipitation (color) and water surface wind (arrows). (f) Boreal summer δ^{18}O of precipitation (color) and surface wind (arrows). Filled and open stars in Figure 1a indicate locations where MH-LH δ^{18}Osw differences estimated by sediment data are and are not, respectively, statistically significant (Table 1).

low. However, on longer, orbital time scales, the simulated δ^{18}Osw-salinity relationship changes because of changes in water vapor transported in and out of the Pacific Ocean (Figures 1c and 1d). The water vapor flux out of the region is associated with tropospheric vapor that is significantly more depleted than the freshwater end member associated with the tropical water cycle as a whole. Thus variations in this export flux cause a proportionally larger change in isotope values than seen in the spatial relationship. A northward shift of the boreal summer (and annual mean) Atlantic Intertropical Convergence Zone (ITCZ) paired with weaker Pacific easterlies reduces reduce the amount of low-δ^{18}O water vapor transported across Central America from the Atlantic Ocean (Figure 1d). Stronger boreal summer (and annual mean) easterly winds over the western Pacific (Figure 1f) carry more low-δ^{18}O water vapor from the Pacific to the Indian Ocean. These changes in water vapor transport increase the δ^{18}O of precipitation in the western tropical Pacific by ~0.5 to 1‰ in the annual mean, depending on location.

[13] Despite reduced Atlantic-to-Pacific water vapor transport, there is an increase in boreal summer (and mean annual) precipitation in the eastern Pacific (Figure 1d) and a decrease in the δ^{18}O of precipitation (Figure 1f), just west of the Isthmus of Panama. These changes occur even though there is less cross-Isthmus water vapor transport because easterly surface winds weaken and export less vapor to the western Pacific, enhancing moisture convergence in the east. Only one sediment core from the Caribbean Sea has data that span the Holocene to test for a decrease in evaporation and correspondingly, in δ^{18}Osw, but it is from the Cariaco Basin, where surface properties are strongly influenced by localized upwelling [*Lea et al.*, 2003] that cannot be resolved by the model.

[14] The decrease in water vapor transport from the Atlantic Ocean and the increase in water vapor transport to the Indian Ocean raise the mean salinity of the Pacific Ocean. Other oceanic and atmospheric processes increase the western Pacific salinity and δ^{18}Osw further. In the MH simulation, positive precipitation anomalies occur over land, especially over East Asia and India, and negative precipitation anomalies (approximately 0.4 mm/day) occur over much of the warm waters of the western Pacific and northern Indian Oceans (Figure 1d). This redistribution of moisture from the western Pacific during the LH to the Asian landmass during the MH is a result of the greater intensity of the summer monsoon.

[15] Finally, advection of salt to the western Pacific by surface currents was greater in the MH simulation (Figure 1b). A northward shift in tropical surface currents increases salt advection to the region. The South Equatorial Current (SEC) is saltier than during the LH because of overall increased Pacific salinity, and more of it is deflected northward when it encounters New Guinea. In response to stronger winds, tropical surface ocean currents are stronger in the MH simulation, further enhancing the transport of salt into the region by surface currents. Despite reduced precipitation, the western Pacific is still the region of greatest maritime precipitation, and intensified northward currents advect freshwater out of the region.

[16] As already noted, data and model suggest that southwestern Indonesia experienced little change in δ^{18}Osw. During the MH, precipitation increased here due to the intensification of the northwest (boreal winter)

monsoon (Figure 1c) and the δ^{18}O of local precipitation decreased (Figure 1e), rather than increased as over open western Pacific. The model results showing that the core sites are near the transition between the western Pacific region having higher MH salinity and δ^{18}Osw and the Indian Ocean with lower MH salinity and δ^{18}Osw (Figure 1b) implies that the effects of greater MH precipitation with lower δ^{18}O on the local δ^{18}Osw are diminished by ocean dynamics.

6. Broader Implications

[17] Most tropical records indicate a maximum response of the hydrologic cycle at ~9–10 ka [*Fleitmann et al.*, 2003; *Gasse*, 2000; *Haug et al.*, 2001; *Stott et al.*, 2004; *Thompson and Davis*, 2005; *Wang et al.*, 2005], lagging the 11ka boreal summer insolation maximum by 1–2 kyr, rather than during the MH (6 ka). Larger amplitude precession cycles occurred during the last interglacial (~70–130 ka), and precession maxima were associated with greater Asian monsoon intensification and larger positive δ^{18}Osw anomalies in the western Pacific [*Oppo and Sun*, 2005]. Thus, the MH-LH differences implied by the data-model comparison may be smaller than changes that occurred earlier, and as recently as ~9 ka. Furthermore, this study is consistent with the hypothesis that low precession and weak monsoons contributes to reduced δ^{18}Osw, and presumably salinity, in the western Pacific, during glacial periods [*Oppo and Sun*, 2005] and may explain why the glacial-interglacial δ^{18}O amplitude of the western tropical Pacific, as recorded by planktonic foraminifera, is smaller than that of other regions [*Broecker*, 1986]. Millennial time scale western Pacific δ^{18}Osw variations are superimposed on orbital scale variability, but the sign of the correspondence between monsoons and western Pacific δ^{18}Osw is opposite; warm millennial events are associated with both strong monsoons and low western Pacific δ^{18}Osw [*Stott et al.*, 2002]. Other model simulations suggest that during millennial events induced by reduced North Atlantic overturning, summer rainfall is reduced both over the continents and the western Pacific, consistent with paleoclimatic evidence [*Zhang and Delworth*, 2005].

7. Conclusions

[18] Paleoceanographic data from the low latitude Pacific Ocean indicate changes in the freshwater budget and redistribution of freshwater within the basin. Isotope climate model simulations suggest that the relationship between surface δ^{18}Osw and salinity is sensitive to changes in the tropical water cycle, and that MH salinity changes in the western Pacific of ~0.5 to 0.7 psu, or about 65% of that inferred previously. The simulations suggest that several factors influenced the freshwater budget of the low-latitude Pacific Ocean during the MH, including changes in moisture transport in and out of the Pacific, changes in ocean currents, and a redistribution of precipitation from the western Pacific to the Asian landmass.

8. Appendix: Data-Model SST Comparisons

[19] Mg/Ca-based SST estimates suggest slightly cooler conditions during the MH in the eastern tropical Pacific and north-western subtropical Pacific and slightly warmer in the western tropical Pacific (Table 1). The simulations suggest that the tropics, including the western Pacific were cooler during the MH, consistent with most [*Kitoh and Murakami*, 2002; *Gladstone et al.*, 2005; *Masson-Delmotte*, 2006] but not all [*Liu et al.*, 2003] previous MH simulations. Because of the generally cooler western Pacific, most models simulate a reduction in precipitation over the region. On the other hand, a warmer western tropical Pacific causes enhanced convection over the region and the fresher conditions reported by *Abram et al.* [2007]. One factor that may complicate interpretations may be shifts in El Niño Southern Oscillation (ENSO) phase and/or frequency that models do not capture consistently. In GISS ModelE, relatively coarse tropical ocean resolution precludes the simulation of realistic ENSO variability and is associated with an insufficient east-west tropical Pacific SST gradient in the LH simulation. Additional work is needed to reconcile the paleoceanographic data suggesting both warmer conditions and fresher surface waters at 6k and model results that show a close coupling between SST and local convection (and presumably salinity). However, in both the models and the data, the SST differences are small (<0.5°C) compared to the air temperature increase over Asia (1.5–2.5°C), which increases the land-sea temperature contrast [see *Schmidt et al.*, 2007, Figure 7]. General agreement with the surface δ^{18}Osw may suggest that changes in the hydrologic cycle are reasonably well simulated if the sense of the changes in land-sea temperature contrast is simulated. However, the SST mismatch may contribute to underestimation of the δ^{18}Osw changes in the model simulations. Applying an equation to the published Mg/Ca that implies a smaller exponential increase in Mg/Ca for a 1°C SST increase [*McConnell and Thunell*, 2005] would increase the data-model discrepancies for both SST and δ^{18}Osw.

[20] **Acknowledgments.** We thank W. Curry and A. Carlson for discussions, A. Koutavas, D. Lea, L. Stott, and R. Thunell for providing their published data in digital form, and L. Stott and R. Thunell for their helpful reviews. We acknowledge the international modeling groups for providing their data for analysis, the Laboratoire des Sciences du Climat et de l'Environnement (LSCE) for collecting and archiving the model data. The PMIP2/MOTIF Data Archive is supported by CEA, CNRS, the EU project MOTIF (EVK2-CT-2002-00153) and the Programme National d'Etude de la Dynamique du Climat (PNEDC). The analyses were performed using version 02-20-2007 of the database. More information is available on http://www-lsce.cea.fr/pmip/ and http://www-lsce.cea.fr/motif/ . This work was supported by NSF grants ATM-0501241, ATM-0501351, and WHOI's Ocean and Climate Change Institute.

References

Abram, N. J., M. K. Gagan, Z. Liu, W. S. Hantoro, M. T. McCulloch, and B. W. Suwargadi (2007), Seasonal characteristics of the Indian Ocean Dipole during the Holocene epoch, *Nature*, *445*, 299–302.

Bemis, B. E., H. J. Spero, J. Bijima, and D. W. Lea (1998), Reevaluation of the oxygen isotopic composition of planktonic foraminifera: Experimental results and revised paleotemperature equations, *Paleoceanography*, *13*, 150–160.

Berger, A. (1978), Long-term variations of daily insolation and Quaternary climatic changes, *J. Atmos. Sci.*, *35*, 2362–2367.

Broecker, W. (1986), Oxygen isotope constraints on surface ocean temperatures, *Quat. Res.*, *26*, 121–134.

Dekens, P. S., D. W. Lea, D. K. Pak, and H. J. Spero (2002), Core top calibration of Mg/Ca in tropical foraminifera: Refining paleotemperature estimation, *Geochem. Geophys. Geosyst.*, *3*(4), 1022, doi:10.1029/2001GC000200.

Fleitmann, D., S. J. Burns, M. Mudelsee, U. Neff, J. Kramers, A. Mangini, and A. Matter (2003), Holocene forcing of the Indian monsoon recorded in a stalagmite from southern Oman, *Science*, *300*, 1737–1739.

Gagan, M. K., L. K. Ayliffe, D. Hopley, J. A. Cali, G. E. Mortimer, J. Chappell, M. T. McCulloch, and J. M. Head (1998), Temperature and surface ocean water balance of the mid-Holocene tropical western Pacific, *Science*, *279*, 1014–1018.

Gasse, F. (2000), Hydrological changes in the African tropics since the Last Glacial Maximum, *Quat. Sci. Rev.*, *19*, 189–211.

Gladstone, R. M., et al. (2005), Mid-Holocene NAO: A PMIP2 model intercomparison, *Geophys. Res. Lett.*, *32*, L16707, doi:10.1029/2005GL023596.

Haug, G. H., K. A. Hughen, D. M. Sigman, L. C. Peterson, and U. Röhl (2001), Southward migration of the Intertropical Convergence Zone through the Holocene, *Science*, *294*, 1304–1308.

Holmgren, K., J. A. Lee-Thorp, G. R. J. Cooper, K. Lundblad, T. C. Partridge, L. Scott, R. Sithaldeen, A. S. Talma, and P. D. Tyson (2003), Persistent millennial-scale climatic variability over the past 25,000 years in southern Africa, *Quat. Sci. Rev.*, *22*, 2311–2326.

Kitoh, A., and S. Murakami (2002), Tropical Pacific climate at the mid-Holocene and the Last Glacial Maximum simulated by a coupled ocean-atmosphere general circulation model, *Paleoceanography*, *17*(3), 1047, doi:10.1029/2001PA000724.

Koutavas, A., J. Lynch-Stieglitz, T. M. Marchitto, and J. P. Sachs Jr. (2002), El Niño-like pattern in ice age tropical Pacific sea surface temperature, *Science*, *297*, 226–230.

Koutavas, A., P. B. deMenocal, G. C. Olive, and J. Lynch-Stieglitz (2006), Mid-Holocene El Niño-Southern Oscillation (ENSO) attenuation revealed by individual foraminifera in eastern tropical Pacific sediments, *Geology*, *34*, 993–996.

Lea, D. W., D. K. Pak, and H. J. Spero (2000), Climate impact of late Quaternary equatorial Pacific sea surface temperature variations, *Science*, *289*, 1719–1724.

Lea, D. W., D. K. Pak, L. C. Peterson, and K. A. Hughen (2003), Synchroneity of tropical and high-latitude Atlantic temperatures over the last glacial termination, *Science*, *301*, 1361–1364.

Lea, D. W., D. K. Pak, C. L. Belanger, H. J. Spero, M. A. Hall, and N. J. Shackleton (2006), Paleoclimate history of Galápagos surface waters over the last 135,000 years, *Quat. Sci. Rev.*, *25*, 1152–1167.

LeGrande, A. N., and G. A. Schmidt (2006), Global gridded data set of the oxygen isotopic composition in seawater, *Geophys. Res. Lett.*, *33*, L12604, doi:10.1029/2006GL026011.

Liu, Z., E. Brady, and J. Lynch-Stieglitz (2003), Global ocean response to orbital forcing in the Holocene, *Paleoceanography*, *18*(2), 1041, doi:10.1029/2002PA000819.

Masson-Delmotte, V. (2006), Past and future polar amplification of climate change: Climate model intercomparisons and ice-core constraints, *Clim. Dyn.*, *26*, 513–529.

McConnell, M. C., and R. C. Thunell (2005), Calibration of the planktonic foraminiferal Mg/Ca paleothermometer: Sediment trap results from the Guaymas Basin, Gulf of California, *Paleoceanography*, *20*, PA2016, doi:10.1029/2004PA001077.

Moy, C. M., G. O. Seltzer, D. T. Rodbell, and D. M. Anderson (2002), Variability of El Niño/Southern Oscillation activity at millennial timescales during the Holocene epoch, *Nature*, *420*, 162–165.

Oppo, D. W., and Y. Sun (2005), Amplitude and timing of sea surface temperature change in the northern South China Sea: Dynamic link to the East Asian Monsoon, *Geology*, *33*, 785–788.

Schmidt, M. W., H. J. Spero, and D. W. Lea (2004), Links between salinity variation in the Caribbean and North Atlantic thermohaline circulation, *Nature*, *428*, 160–163.

Schmidt, G. A., A. N. LeGrande, and G. Hoffmann (2007), Water isotope expressions of intrinsic and forced variability in a coupled ocean-atmosphere model, *J. Geophys. Res.*, *112*, D10103, doi:10.1029/2006JD007781.

Schmittner, A., and A. C. Clement (2002), Sensitivity of the thermohaline circulation to tropical and high latitude freshwater forcing during the last glacial-interglacial cycle, *Paleoceanography*, *17*(2), 1017, doi:10.1029/2000PA000591.

Spero, H. J., and D. W. Lea (2003), The cause of carbon isotope minimum events on glacial terminations, *Science*, *296*, 522–525.

Stott, L. D., C. Poulsen, S. Lund, and R. Thunell (2002), Super ENSO and global climate oscillations at millennial time scales, *Science*, *297*, 222–226.

Stott, L., K. Cannariato, R. Thunell, G. Haug, A. Koutavas, and S. Lund (2004), Decline of surface temperature and salinity in the western tropical Pacific Ocean in the Holocene epoch, *Nature*, *431*, 56–59.

Sun, D., M. K. Gagan, H. Cheng, H. Scott-Gagan, C. A. Dykoski, R. L. Edwards, and R. Su (2005), Seasonal and interannual variability of the Mid-Holocene East Asian monsoon in coral $\delta^{18}O$ records from the South China Sea, *Earth Planet. Sci. Lett.*, *237*, 69–84.

Sun, Y., D. W. Oppo, R. Xiang, W. Liu, and S. Gao (2005), The last deglaciation in the Okinawa Trough: Subtropical northwest Pacific link to Northern Hemisphere and tropical climate, *Paleoceanography*, *20*, PA4005, doi:10.1029/2004PA001061.

Thompson, L. G., and M. E. Davis (2005), Stable isotopes through the Holocene as recorded in low-latitude, high-altitude ice cores, in *Isotopes and the Water Cycle, Past, Present and Future of a Developing Science*, pp. 321–339, Springer, New York.

Visser, K., R. Thunell, and L. Stott (2003), Magnitude and timing of temperature change in the Indo-Pacific warm pool during deglaciation, *Nature*, *412*, 152–155.

Wang, Y. J., et al. (2005), The Holocene Asian monsoon: Links to solar changes and North Atlantic climate, *Science*, *308*, 854–857.

Zhang, R., and T. L. Delworth (2005), Simulated tropical response to a substantial weakening of the Atlantic thermohaline circulation, *J. Clim.*, *18*, 1853–1860.

A. N. LeGrande and G. A. Schmidt, NASA Goddard Institute for Space Studies and Center for Climate Systems Research, Columbia University, 2880 Broadway, New York, NY 10025, USA.

D. W. Oppo, Department of Geology and Geophysics, Woods Hole Oceanographic Institution, 360 Woods Hole Road, MS 23, Woods Hole, MA 02543, USA. (doppo@whoi.edu)